LA-8500-PR

Progress Report

Explosively Produced Fracture of Oil Shale

October—December 1979

University of California

LOS ALAMOS SCIENTIFIC LABORATORY

Post Office Box 1663 Los Alamos, New Mexico 87545

The four most recent reports in this series, unclassified, are LA-8024-PR, LA-8104-PR, LA-8396-PR, and LA-8397-PR.

Edited by

Lidia G. Morales

Photocomposition by

Alice Creek

This work was supported by the US Department of Energy, Office of the Assistant Secretary for Fossil Energy.

LA-8500-PR
Progress Report

UC-91
Issued: February 1981

Explosively Produced Fracture of Oil Shale

October—December 1979

Los Alamos Oil Shale Working Group
W. A. Morris, Project Leader

CONTENTS

EXPLOSIVELY PRODUCED FRACTURE OF OIL SHALE
OCTOBER—DECEMBER 1979

by

Los Alamos Oil Shale Working Group
W. A. Morris, Project Leader

ABSTRACT

A Jones-Wilkins-Lee (JWL) equation of state for ammonium nitrate/fuel oil mixture (ANFO) and aluminized ANFO, somewhat different from the Becker-Kistiakowsky-Wilson (BKW) equation of state described in previous reports, is discussed. Included also are our present understanding of a steady, cylindrical detonation, a proposed computer model of a real detonation, the requirements for an equivalent equation of state to be used with the model, and the values for the equation-of-state parameters. An alternative explosive burn package has been implemented in the computer code YAQUI together with a slip-line capability at the explosive/oil shale interface. The code has been used for prediction of cratering and fragmentation experiment results on a field scale.

EXPLOSIVE CHARACTERIZATION

EQUIVALENT EQUATION OF STATE FOR ANFO AND ALUMINIZED ANFO
(W. C. Davis)

INTRODUCTION

Our goal is to measure detonation properties of blasting explosives and use them in detailed computer calculations that predict effects of the explosive on the surrounding rock. Important properties are the equation of state (eos) of the detonation products and the rate of heat release from chemical reactions. If these properties are known, the behavior of an explosive in any configuration can, at least in principle, be calculated. The calculations, however, are very complicated, and even if they can be done with existing codes, they provide more detail than can be used for any practical purpose. For practical engineering at reasonable cost, the calculation must be reduced in complexity. Our present approach is to use our knowledge of the existing system to produce a calculation procedure that is simpler but that still gives an adequate approximation of the real detonation. Presented in this report are our present understanding of the steady, cylindrical detonation, the proposed computer model of the real detonation, the requirements for an equivalent eos to be used with the model, and values for the eos parameters.

STEADY DETONATION OF A CYLINDRICAL EXPLOSIVE CHARGE

Steady detonation of a cylindrical charge (for example, an explosive in a borehole) has a leading shock wave followed by the chemical reaction and then by the main expansion of the reacted gases. Figure 1 is a diagram of the process. The shock wave is curved, so the streamlines bend outward from the very start, and the pressure just behind the shock is lower at the edge than at the center. The chemical reaction, with its pressure-dependent rate,

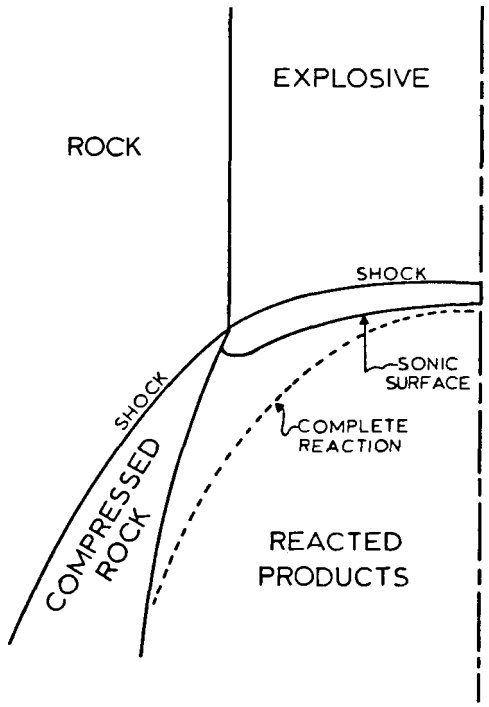

Fig. 1.
Diagram of detonation in a cylindrical borehole.

proceeds more slowly near the edge than at the center. The dashed line in Fig. 1 outlines the surface where the chemical reaction is complete. The flow immediately behind the shock is subsonic relative to the shock, and the flow far behind the shock is supersonic. The dividing surface, or sonic surface, is shown as a solid line in Fig. 1. Detonation velocity is less than that for a plane detonation because some of the chemical energy is not available to drive the wave forward. Some of the chemical energy goes into lateral kinetic energy of the divergent flow, and some of it is not available because energy liberated behind the sonic surface does not go forward to drive the wave. In this description, even though not all the energy is available to drive the detonation wave at full velocity, all the chemical energy is released and is available to drive the rock.

SIMPLE APPROXIMATION TO CYLINDRICAL DETONATION

If the computer programs could do the calculation required for Fig. 1, they could use the exact eos and rate law. Then the calculation of the motion of the rock would be precisely correct for any size borehole. Unfortunately, they cannot. An adjusted rather than exact rate and eos could be used in a simpler calculation so that the end result, the calculation of the rock motion, would be an acceptable approximation. Therefore, it seems best to use a model for the detonation that is independent of calculational details.

A simple approximation to the detonation is diagrammed in Fig. 2. The reaction rate is assumed to be infinite, so the shock, sonic surface, and complete-reaction surface are all coincident. The detonation can be put into the calculation as a moving step at the proper velocity or can be modeled by a fast, plane, artificial reaction that approximates the instantaneous reaction. Then the main calculation is for an inert flow, using an eos for the reacted products.

For this system to work, the eos has to give the exact sonic flow at the detonation velocity for the size of cylinder. It must also give the proper product energy that transfers to the rock.

REQUIREMENTS FOR AN EQUIVALENT EQUATION OF STATE OF ANFO

The requirements for the equivalent eos are

(1) the observed detonation velocity $D = D(R)$, where R is the cylinder radius of the explosive, must take the material to the sonic point,

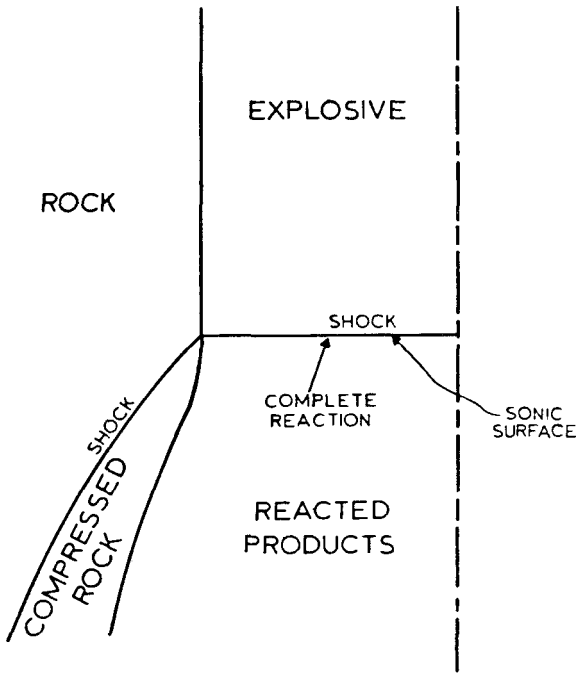

Fig. 2.
Simple approximation to detonation in a borehole.

(2) energy delivered to the rock must agree with observation,
(3) the total energy released at full expansion must equal the total chemical energy released in the reaction, and
(4) the Chapman-Jouquet (CJ) pressure at infinite radius must agree with the measurements made on large, plane detonations.

Preliminary analysis of the available detonation velocity measurements indicates that the velocity is given by the following confinements:

copper $D = 4.78 - 40/R$, $R_f = 24$ mm
rock $D = 4.78 - 65/R$, $R_f = 38$ mm
Plexiglas $D = 4.78 - 75/R$, $R_f = 46$ mm

where D is given in mm/μs or km/s, R is the cylinder radius in mm, and R_f is the failure radius below which the explosive will not detonate. All these values are adjusted for ANFO at a density of 0.85 g/cm³.

One measure of the energy delivered by the explosive is the standard cylinder test. There are a few experiments that have been done for ANFO by Lawrence Livermore National Laboratory (LLNL). The very limited data are fit by

$$V_{19} = 0.901 - \frac{58}{R^2} ,$$

where V_{19} is the velocity of the copper wall in mm/μs after expansion to 19 mm (a standard terminology), and R is the charge radius in mm. The data do not justify this fit, which was chosen after the interpretation of experiment data of other explosives.

The chemical energy released by complete reaction of ANFO is 3.8 MJ/kg. It is widely believed that the reaction does not go to completion, and that perhaps an eighth of the available energy is not released. We will therefore use 3.3 MJ/kg as an approximate value.

A few of our measurements indicate that the CJ pressure for an infinite medium is ~0.060 Mbar. The density fit to apparent values of gamma is

$$\gamma = 1.6 + 0.8\rho_o ,$$

where ρ_o is the density. For $\rho_o = 0.85$, $\gamma = 2.28$. The CJ relation

$$p = \frac{\rho_o D^2}{\gamma + 1} ,$$

where p is the pressure, then gives a CJ pressure of 0.059 Mbar for D = 4.78.

PROVISIONAL EQUIVALENT EQUATION OF STATE FOR ANFO—JONES-WILKINS-LEE (JWL) FORM

The JWL eos has two main advantages for our present purposes. It has six constants, enough to allow calibration, but not so many as to make the calibration completely arbitrary. Also, most computer routines can use it without additional coding. Its disadvantage is its ad hoc form, which makes it impossible to relate it to the physics of the molecular interactions and the oscillatory shape of the γ vs volume curve.

The centimeter-gram-microsecond system of units is always used with the JWL eos. Thus at the CJ state, the detonation velocity D is 0.478 cm/μs, and with $\gamma = 2.28$, the CJ pressure is 0.0592 Mbar. The relative volume $V_j = 0.695$, the explosive energy $e_o = 0.02805$ Mbar-cm³/cm³, and the density $\rho_o = 0.85$ g/cm³.

The calibration is done by setting the energy, pressure, and slope of the isentrope to the CJ values. The equations are

$$e_o + \frac{1}{2}\rho_o D^2(1 - V_j)^2 = \left(\frac{a_1}{R_1}\right)A + \left(\frac{a_2}{R_2}\right)B + \left(\frac{a_3 V_j}{w}\right)C , \quad (1)$$

$$\rho_o D^2(1 - V_j) = a_1 A + a_2 B + a_3 C , \quad (2)$$

and

$$\rho_o D^2 = a_1 R_1 A + a_2 R_2 B + \left[a_3 \frac{1 + w}{V_j C}\right] , \quad (3)$$

where A, B, C, R_1, R_2, and w are constants and

$$a_1 = \exp(-R_1 V_j) \qquad a_2 = \exp(-R_2 V_j)$$

$$a_3 = V_j^{-w-1} . \quad (4)$$

To give the JWL eos about the desired form, we choose $R_1/R_2 = 4$ and w = 0.3. Then any choice of R_1 results in

a set of linear algebraic equations in A, B, and C. Inversion of the matrix can be done easily.

The choice of a particular value for R_1 is made by requiring that the energy given to the cylinder wall in the standard cylinder test comes out right. This can be achieved by making the energy of the Fickett-Jacobs diagram truncated at $V = 3.3$ equal to the Gurney energy calculated from the cylinder test. The Gurney energy is given by

$$e_G = \left(\frac{M}{A}\right)\left(\frac{1}{2}V_{19}^2\right)\left[1 + \frac{1}{2}\rho_o\left(\frac{M}{A}\right)\right] , \qquad (5)$$

where $M = 19.501$ g/cm is the mass of the standard copper tube, and $A = 5.067$ cm^3/cm is the area of the tube. The data extrapolate to $V_{19} = 0.0901$ cm/μs for the infinite size. The Gurney energy $e_G = 0.01735$ Mbar-cm^3/cm^3 is the area of the truncated diagram, and e_o is the area of the whole diagram. Thus $e(3.3) = e_o - e_G = 0.01070$. This energy is obtained from the energy equation

$$e = \left(\frac{A}{R_1}\right)\exp(-R_1V) + \left(\frac{B}{R_2}\right)\exp(-R_2V) + \left(\frac{C}{w}\right)V^{-w} . \qquad (6)$$

By iterating with different values of R_1, one can satisfy the condition $e(3.3) = 0.01070$ Mbar-cm^3/cm^3.

The results of the calibration are

$R_1 = 4.20$ $R_2 = 1.05$ $w = 0.3$
$A = 0.74373$ $B = 0.02540$ $C = 0.00427$.

This calibration is for the extrapolation to infinite charge size. It gives the wrong detonation velocity for finite charges and slightly too much energy to the surroundings.

For finite diameter charges, an equivalent eos is needed. The procedure to calibrate it is almost the same as for the CJ eos, except that the equivalent CJ point for the equivalent eos is not a real physical state but one chosen to fit the data. Therefore, we fix R_1 at the value found above and adjust the eos by varying the equivalent V_j. The equations are Eqs. (1) through (5). The Gurney energy is taken from the fit to the cylinder test results for each detonation velocity. For each detonation velocity, there is a calibration for the parameters of the eos. These are fit to a quadratic curve for convenience of presentation. The final calibration for ANFO at initial density 0.85 g/cm^3 is

$R_1 = 4.20$ $R_2 = 1.05$ $w = 0.3$
$V_j = 0.4239 + 0.6840D - 0.2433D^2$
$A = 0.4624 - 3.915D + 9.420D^2$
$B = -0.1027 + 0.5997D - 0.6939D^2$
$C = 0.01853 - 0.06005D + 0.06321D^2$

Plots of the isentropes are given in Figs. 3 and 4.

The isentropes must be related to the diameter of the explosive charge by the detonation velocity vs radius data. We assume that the eos depends only on detonation velocity and not on the other parameters of confinement. The confinement data are

copper $D = (\text{cm}/\mu\text{s}) = 0.478 - 0.80/\text{diam (cm)}$
rock or clay $D = (\text{cm}/\mu\text{s}) = 0.478 - 1.30/\text{diam (cm)}$
Plexiglas $D = (\text{cm}/\mu\text{s}) = 0.478 - 1.50/\text{diam (cm)}$.

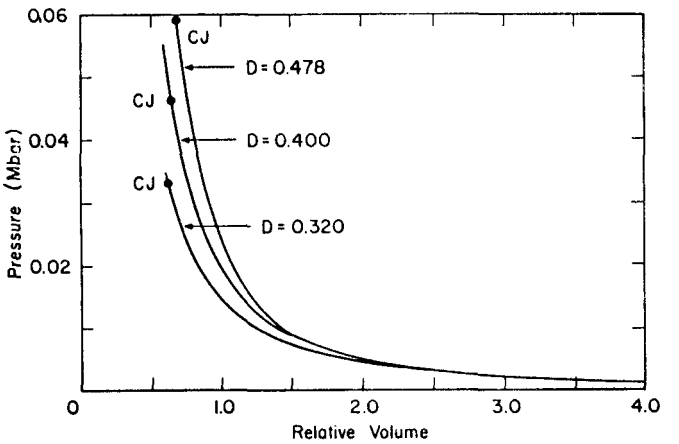

Fig. 3.
Equivalent expansion isentropes for finite diameter charges of ANFO at three detonation velocities at low relative volumes.

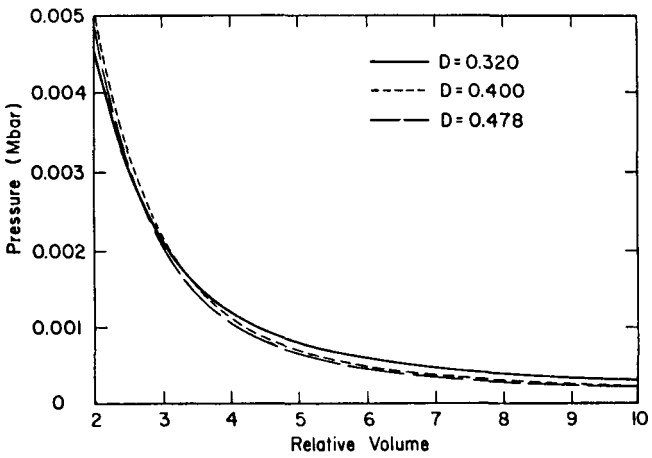

Fig. 4.
Equivalent expansion isentropes for finite diameter charges of ANFO at three detonation velocities at high relative volumes.

APPENDIX

THE JWL EQUATION OF STATE

The JWL isentrope is usually written

$$P = A \exp(-R_1 V) + B \exp(-R_2 V) + C V^{-1-w} ,$$

where p is the pressure on the isentrope, $V = v/v_o$ is the volume on the isentrope relative to the initial volume of the explosive, and A, B, C, R_1, R_2, and w are constants. R_1 is chosen a few times larger than R_2 so that the first term is important at high pressures, the second at middle pressures, and the third at low pressures.

Integrating the isentropic equation $de = -pdV$ gives the energy on the isentrope

$$e = \left(\frac{A}{R_1}\right)\exp(-R_1 V) + \left(\frac{B}{R_2}\right) \exp(-R_2 V) + \left(\frac{C}{w}\right) V^{-w} ,$$

with the constant of the integration chosen to make the energy go to zero at infinite volume.

The energy from the isentrope is usually obtained by eliminating C between the two equations to obtain

$$e = \frac{pV}{w} + A\left(\frac{V}{w} - \frac{1}{R_1}\right)\exp(-R_1 V) + B\left(\frac{V}{w} - \frac{1}{R_2}\right)\exp(-R_2 V) .$$

Notice that the first term is the polytropic gas eos to which the JWL goes at large volume.

The slope of the isentrope, found by differentiation, is

$$\left(\frac{\partial p}{\partial V}\right)_s = -AR_1 \exp(-R_1 V) - BR_2 \exp(-R_2 V) - (1 + w)CV^{-w-2} .$$

At the CJ point, the slope of the isentrope and the slope of the Rayleigh line $-\rho_o D^2$ are equal. This expression for the slope also allows us to find the isentropic exponent

$$\gamma = -\left(\frac{V}{p}\right)\left(\frac{\partial p}{\partial V}\right)_s$$

along the isentrope. The form of the eos gives γ an oscillatory form that is nonphysical, but that does not cause problems in any of the usual applications.

A general discussion of eos's and particular references to the JWL form are given in Ref. 1.

A COMPARISON OF COMPUTER-MODELED HIGH EXPLOSIVE BURN WITH THE SELF-SIMILAR TAYLOR WAVE

(L. G. Margolin)

A high explosive burn package has been added to a version of the YAQUI stress wave propagation computer code. The package includes a slip-line capability at the explosive/medium interface and an algorithm for chemical energy release to simulate burn. A calculation with YAQUI has been compared with the analytic solution for the ideal reactive shock (Taylor wave). The comparisons show excellent agreement between the computer-generated solution and the theoretical solution.

In calculating the hydrodynamics of two materials, the boundary condition at the material interface may be either nonslip or free-slip. Nonslip means that both the normal and the tangential components of velocity must be continuous across the interface. Free-slip means that only the normal component of velocity must be continuous across the interface. In general, it is appropriate to use a nonslip condition for viscous flow and a free-slip condition for inviscid flow.

Consider the case of a detonated column of high explosive contained in oil shale. The thickness of the viscous boundary can be estimated as being three orders of magnitude smaller than either the diameter of the column or the width of a computational cell. Thus, it is appropriate to characterize the interface as a free-slip surface. In the computer code, such an interface is termed a *slip line*.

The tangential component of velocity may vary significantly across a free-slip surface. The following values are typical for a high explosive (ANFO) burn in oil shale. Just behind the burn front, the high explosive will reach velocities of $\sim 8.0 \times 10^4$ cm/s. At the same point, but in the shale, the velocities are $\sim 4.0 \times 10^3$ cm/s—smaller by a factor of about 20. If the interface were treated as a nonslip surface, then each cell vertex lying on the interface would have to represent both these velocities simultaneously with just one value. The result would be a nonphysical coupling of energy from the explosive to the shale by shearing of the cells along the interface.

To complete the burn package, it is necessary to represent the release of the chemical energy of burn. This is done in YAQUI by the use of a burn line, that is, a line which progresses up the column of explosive with the experimentally measured burn-front velocity. In each time step, the volume of explosive passed by the burn line is "burnt" by the deposition of energy equal to the mass of the volume times the measured energy release per unit mass. The method has been generalized to account for the possibility of delayed burn behind the front as discussed by Mader.[2]

To check the burn package, a problem was run with YAQUI in which the shale density was set at 2000 g/cm^3 so that the explosive would be a rigidly confined one and all the energy would be released at the burn front. This problem is the one-dimensional reactive wave, or Taylor wave. An analytic solution to this problem can be constructed from similarity methods.[3] Comparisons between the analytic solution and the computer-generated solution are shown in Figs. 5-8. The computer solution shows the rounding of the sharp maxima that is characteristic of numerical methods. Otherwise, there is very little numerical diffusion or smearing, and agreement appears excellent.

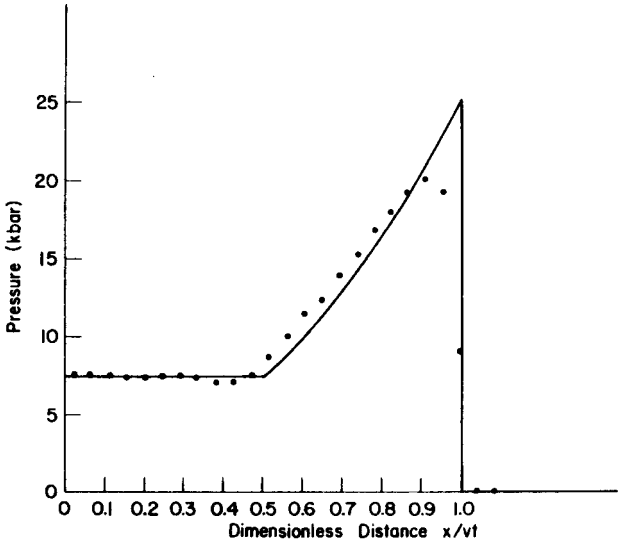

Fig. 5.
Density profiles from analytic theory (solid line) and computer results (dots) for the self-similar Taylor wave.

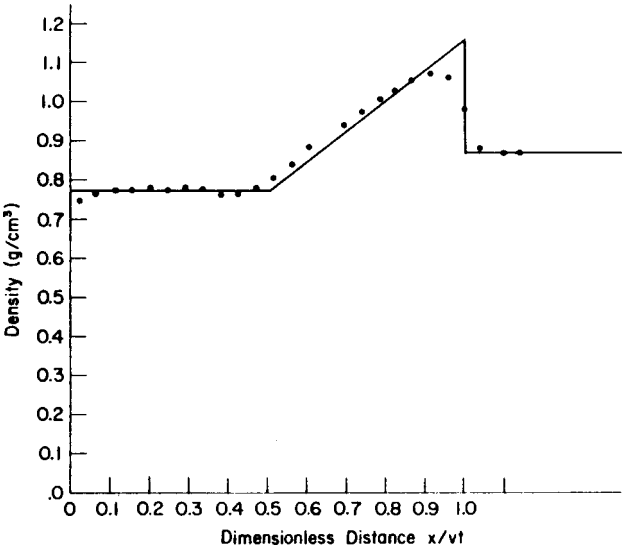

Fig. 7.
Pressure profiles from analytic theory (solid line) and computer results (dots) for the self-similar Taylor wave.

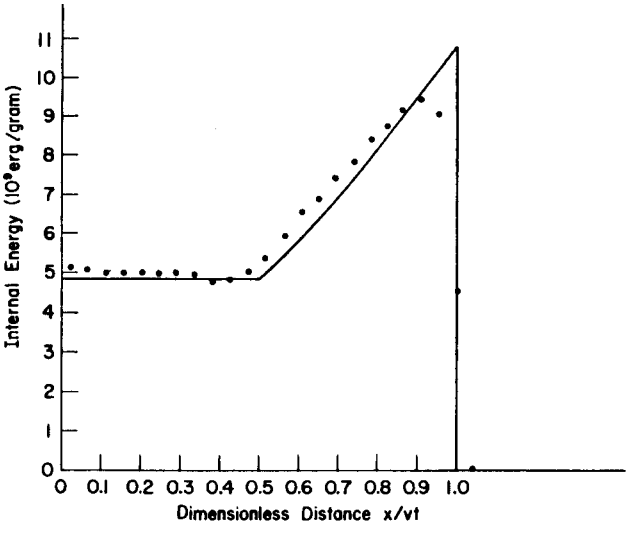

Fig. 6.
Material velocity profiles from analytic theory (solid line) and computer results (dots) for the self-similar Taylor wave.

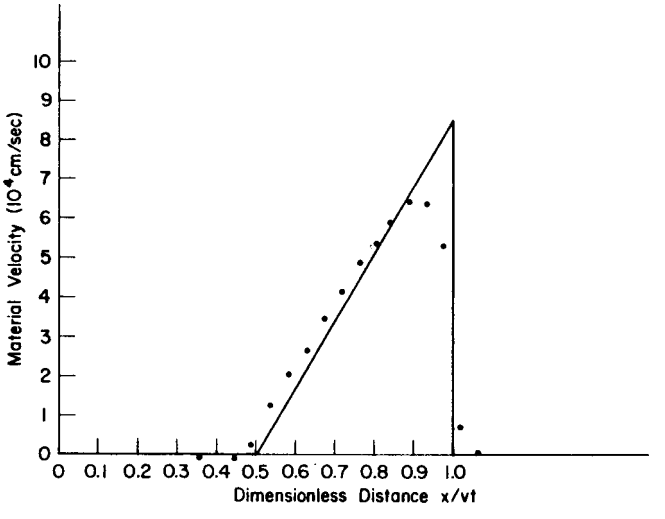

Fig. 8.
Internal energy profiles from analytic theory (solid line) and computer results (dots) for the self-similar Taylor wave.

COMPUTER SIMULATION OF OIL SHALE FRAGMENTATION EXPERIMENTS

(T. F. Adams)

INTRODUCTION

The YAQUI code is an explicit, finite difference, stress wave propagation code that was used for predicting the extent of the damaged or rubbled region for five proposed single-borehole explosive tests in oil shale. These calculations primarily aid in the design of suitable field experiments as part of the larger program to develop and optimize techniques for the explosive rubbling of oil shale.

The calculations have been made with the assumption that ANFO is the explosive used in each of the experiments and that it is loaded into a 0.15-m-diam borehole. It is assumed that the boreholes will be drilled straight down into the mine floor so that the charge will be perpendicular to the free surface. The charges are to be detonated from the bottom so that the explosive will generate a shock wave traveling upward toward the free surface. The charge lengths and depths of burial (DOB) for the proposed experiments are given in Table I.

COMPUTATIONAL METHODS

The nonideal behavior of the explosive is simulated in the calculations by the use of the eos for the detonation products for 0.15-m-diam ANFO published by Craig et al.[4] This eos was determined empirically by matching theoretical calculations with data from actual explosive tests. The traveling detonation front is implemented in the code with a "sharp-shock programmed burn" similar to that described by Mader.[2]

The oil shale is modeled as an elastic/plastic solid with fracture. The material constants used in the calculations are given in Table II. The fracture is simulated with a scalar "damage model," similar to one developed by J. N. Johnson.[5] According to this model, each computational cell has associated with it a damage parameter, D. D varies from zero, the intact oil shale, to a one for fully fractured rock. As D increases, the yield strength γ (in terms of the second invariant of the stress) drops according to the expression

$$Y(P,D) = Y_o\left[1 - D\left(1 - \frac{p}{p^*}\right)^2\right] + \Delta Y\left[1 - \exp\left(\frac{-p}{p_o}\right)\right] .$$

In this expression, p^* is a pressure associated with the brittle-ductile transition. During those time intervals when plastic flow is occurring, D increases according to the expression.

$$\dot{D} = \xi\lambda(1 - D)\left(1 - \frac{p}{p^*}\right) .$$

TABLE I

DESIGN PARAMETERS FOR FIVE OIL SHALE BLASTING EXPERIMENTS

Experiment	Charge Length (m)	DOB (Charge Center) (m)
1	1.00	4.00
2	1.00	2.80
3	1.00	1.50
4	1.70	2.45
5	2.64	1.98

TABLE II

CONSTANTS FOR OIL SHALE USED IN THE YAQUI CALCULATIONS

Quantity	Value
Initial Density	2.3 Mg/m^3
Young's Modulus	0.257 Mbar
Shear Modulus	0.1048 Mbar
High-Pressure Bulk Modulus	0.1584 Mbar
Poisson's Ratio	0.226
Gruneisen Coefficient	1.4
Yield Surface Parameters[a]	
Y_o	0.69 kbar
ΔY_o	4.7 kbar
p_o	3.0 kbar
Brittle/Ductile Transition Pressure[a]	5.0 kbar
Damage Growth Rate Coefficient[a]	20.0 Mbar

[a]See Ref. 5 for definitions.

In this expression, λ is the Lagrange multiplier from the elastic/plastic calculation of the stress rate, and ξ is a constant. The constants used in the damage calculations are given in Table II. The damage model used in the present calculations is a different elastic/plastic model than that described by Johnson.[5] The present calculations were made with a rate-independent plastic flow law with no plastic dilatancy, whereas Johnson's plasticity included time-dependent relaxation (after exceeding the failure criterion) and dilatant behavior. Contour plots of D at various times in the calculations show the extent of the damaged or rubbled region.

The YAQUI calculations for the first four proposed experiments were run long enough to follow the detonation of the explosive and the propagation of the significant shock waves and tensile relief waves through the region of the experiment. Experiments 1, 2, and 4 were run 2.0 ms, whereas experiment 3 only had to be run 1.6 ms because of its shallower DOB. The calculation for experiment 5 terminated prematurely after 1.1 ms because of a technical problem, but by this time, it was already clear that intense rubbling had occurred all the way to the surface and that a crater had been formed. The damage patterns at the end of each of the calculations are shown in Figs. 9-13. Two damage levels are shown in each figure, one at $D = 0.005$, representing the full extent of the rubbling, and one at $D = 0.5$, defining the region of most intense rubbling.

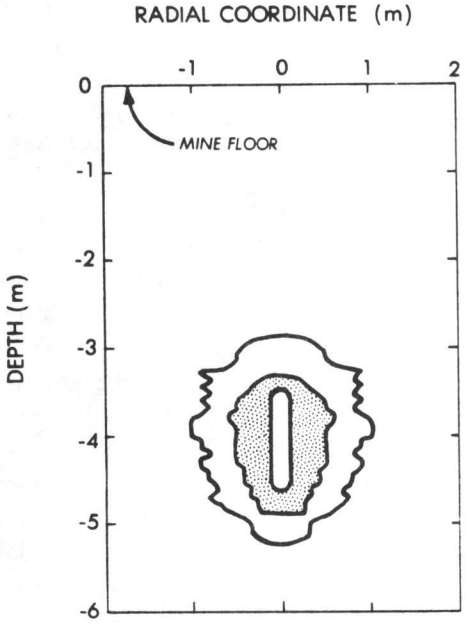

Fig. 9.
Damage contours for proposed experiment 1 at 2.0 ms. The location of the expanded borehole is shown, surrounded by damage contours at the 0.5 level (intense rubbling) and at the 0.005 level (incipent rubbling).

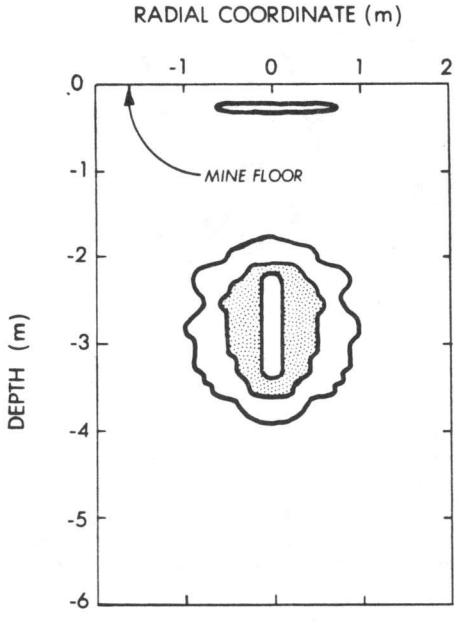

Fig. 10.
Damage contours for proposed experiment 2 at 2.0 ms with the expanded borehole and damage contours at the 0.5 and 0.05 levels.

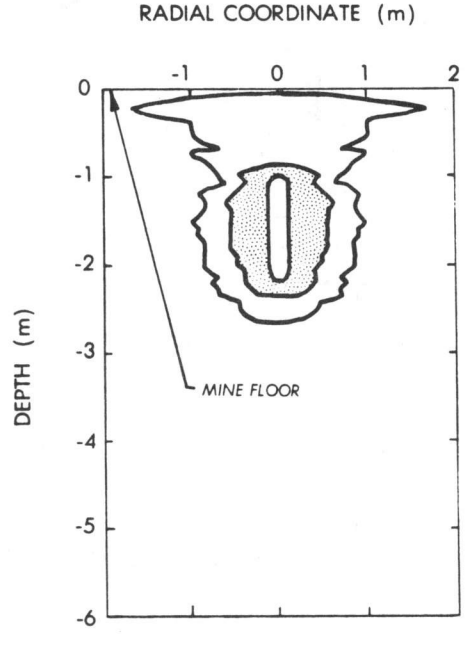

Fig. 11.
Damage contours for proposed experiment 3 at 1.6 ms with the expanded borehole and damage contours at the 0.5 and 0.05 levels.

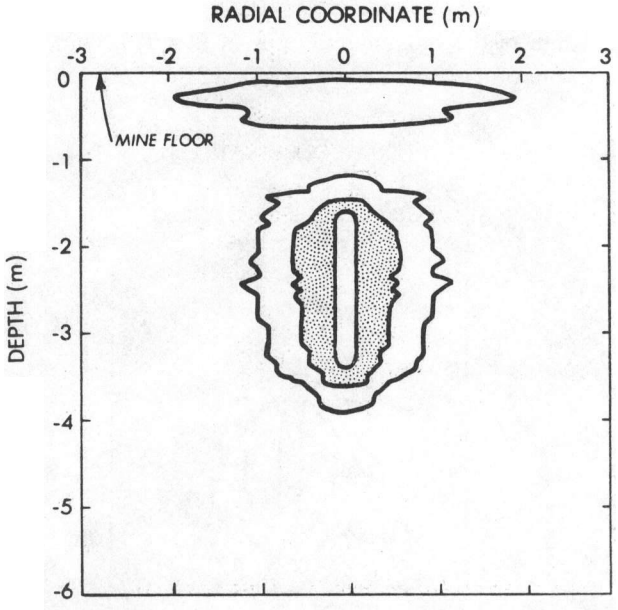

Fig. 12.
Damage contours for proposed experiment 4 at 2.0 ms with the expanded borehole and damage contours at the 0.5 and 0.005 levels.

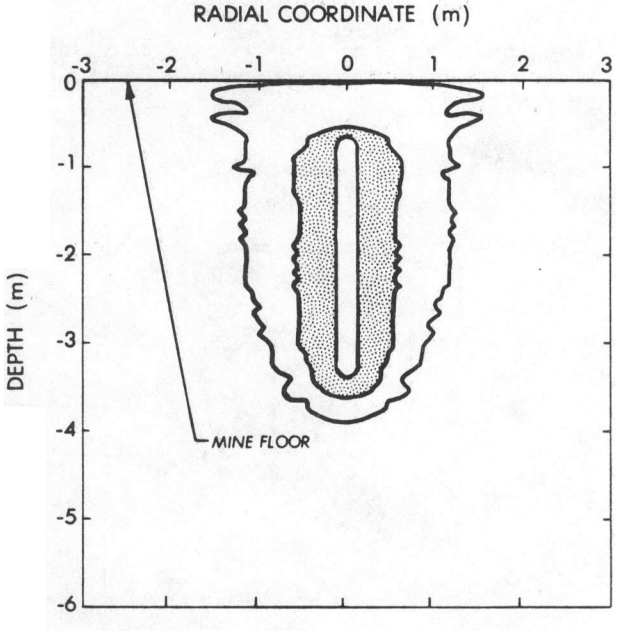

Fig. 13.
Damage contours for proposed experiment 5 at 1.1 ms with the expanded borehole and damage contours at the 0.5 and 0.005 levels.

DISCUSSION

The purpose of the calculations is to provide guidance for planning a field experiment. It is therefore very useful to compare the various proposed experiments to each other. Experiments 1, 2, and 3 all involve a 1-m-long charge but at different DOBs. Experiment 1 is clearly overburied according to Fig. 9 as the damage is entirely confined to the region of the charge. In experiment 2, the charge is closer to the surface, and some incipient surface spall is evident there (Fig. 10). Finally, in experiment 3 (Fig. 11), the charge is close enough to the surface for a significant spall layer to be created. This spall layer, coupled with the damage near the charge, effectively forms the crater that would be produced in this experiment.

Proposed experiments 2, 4, and 5 also show a logical sequence. In each of these experiments, the bottom of the charge lies at 3.33 m. In experiment 2, the charge is only 1 m in length, and as noted, only an incipient spall layer results. In experiment 4, the charge length is now 1.7 m, that is, the borehole is half full. The increased size of charge and shallower effective DOB cause a much more extensive spall layer to be formed. It is not possible to say from this calculation alone whether the field experiment damage pattern would create a crater because preexisting fractures and late-time gas effects could be influential. However, the calculations should be adequate to predict the relative difference between the large spall layer in this experiment and the incipient spall in experiment 2. Finally, in experiment 5, the borehole is loaded almost to the free surface. With such a large charge, it is not surprising that the damage at the surface no longer appears as a separated spall layer, but is effectively an extension of the damage near the charge. This experiment is in the "airblast" region with sufficient energy released to generate appreciable fly rock.

These calculations provide necessary guidance for planning field experiments. They allow planners to make an estimate of the critical DOB, extent of surface spall, and generation of fly rock. The calculations also provide the time histories of stress and velocity at locations throughout the region of the experiment. This additional information can be used to plan appropriate diagnostic instrumentation.

Calculations such as those presented here must be calibrated by a comparison with actual field experiment data. Such a comparison is in progress using the results of blasting experiments in oil shale in the Colony Mine. In the meantime, code calculations can be useful for engineering and planning purposes and as a means to study the basic phenomenology of blasting.

REFERENCES

1. W. Fickett and W. C. Davis, *Deformation* (University of California Press, Berkeley, California, 1979).

2. C. L. Mader, *Numerical Modeling of Detonations* (University of California Press, Berkeley, 1979), pp. 318-319.

3. F. H. Harlow and A. A. Amsden, "Fluid Dynamics—A LASL Monograph," Los Alamos National Laboratory report LA-4700 (June 1971).

4. B. G. Craig, J. N. Johnson, C. L. Mader, and G. F. Lederman, "Characterization of Two Commercial Explosives," Los Alamos National Laboratory report LA-7140 (May 1978).

5. J. N. Johnson, "Calculation of Explosive Rock Breakage: Oil Shale," Proc. 20th U.S. Symp. Rock Mech., Austin, Texas, June 4-6, 1979 (U.S. National Committee for Rock Mechanics, 1979), pp. 109-118.

EXTERNAL DISTRIBUTION

US Department of Energy
Office of Deputy Assistant Secretary
Oil, Gas, and Shale Technology
Mail Stop D-107
Washington, DC 20545
Attn: M. R. Adams
B. DiBona
B. Harney
A. M. Hartstein
J. W. Ramsey
D. Uthus
H. E. Thomas

Laramie Energy Technology Center
P.O. Box 3395, University Station
Laramie, WY 82071
Attn: R. J. Jiacoletti
J. H. Weber
N. Merriam
G. F. Dana
A. E. Harak
W. E. Little
V. Smith
L. P. Jackson
B. Sudduth
J. Edl

Carbondale Mining and Technology Center
Carbondale, IL 62901
Attn: C. Hayduk
T. Ziegler

Sandia Laboratories
Albuquerque, NM 87115
Attn: H. M. Stoller, Org. 5730
A. L. Stevens, Org. 5734
B. Bader, Org. 4737
D. E. Grady, Org. 5163
B. M. Butcher, Org. 5163
K. W. Schuler, Org. 5163
R. A. Schmidt, Org. 5163
M. E. Kipp, Org. 5162
L. D. Bertholf, Org. 5162

Lawrence Livermore Laboratory
University of California
P.O. Box 800
Livermore, CA 94550
Attn: A. E. Lewis, L-207
R. N. Schock, L-437
D. B. Larson, L-205
Merle E. Hanson, L-200
Jon B. Bryan, L-200
Andre Kusabow, L-205
Jack Campbell, L-207

Lawrence Berkeley Laboratory
One Clyclotron Road
Berkeley, CA 94720
Attn: P. Fox

P. G. Wapner
Gulf Mineral Resources Corp.
1780 S. Bellaire St.
Denver, CO 80220

SRI International
333 Ravenswood Ave.
Menlo Park, CA 94025
Attn: D. R. Curran
William Murri
D. Shockey
S. McHugh
L. Seaman
D. Keough

University of Minnesota
Department of Civil and Mineral Engineering
112 Mines and Metallurgy Building
Minneapolis, MN 55455
Attn: Charles Fairhurst

US Bureau of Mines - Twin Cities
P.O. Box 1660
Twin Cities Airport, MN 55111
Attn: Richard Thill
William Olsson

Denver Mining Research Center
US Bureau of Mines
Building 20, Denver Federal Center
Denver, CO 80225
Attn: Paul L. Russell
W. R. Nicholls
V. E. Hooker
Stephen Utter

Systems Science, and Software
Box 1620
La Jolla, CA 92038
Attn: T. Blake
C. Peterson
T. Cherry

Science Applications
1250 Prospect St.
La Jolla, CA 92067
Attn: Elgie McGrath
David Bernstein

Science Applications
8210 Capwell Drive
Oakland, CA 94621
Attn: Ronald Hofmann

Sidney Green
Terra Tek, Inc.
University Research Park
420 Wakara Way
Salt Lake City, UT 84108

William Bergen
Mobil Research and Development
Princetown, NJ 08540

Occidental Exploration and Production
5000 Stockdale Highway
Bakersfield, CA 93309
Attn: Thomas E. Ricketts

D. Zerga
Geokinetics, Inc.
288 Buchanan Field Road
Concord, CA 94520

Fred S. Reynolds
Suite 2908
Fort Worth National Bank Building
Fort Worth, TX 76102

Cameron Engineering
Oil Shale Division
1315 S. Clarkston St.
Denver, CO 80210

Fun Den Wang, Director
Excavation, Engineering, and Earth
Mechanics Institute
Colorado School of Mines
Golden, CO 80401

Capt. Gordon F. Lederman, Jr.
AFWL-DEDIA
Kirtland AFB, NM 87117

J. E. Virgona
2784 Crossroads Blvd., Rm. 110
Grand Junction, CO 81501

Occidental Research Corporation
1855 Carrion Road
La Verne, CA 91750
Attn: Allen Sass
Robert E. Lumpkin

Bureau of Mines - Spokane
East 315 Montgomery St.
Spokane, WA 99205
Attn: John Corwine, Research Director
Ernest L. Corp

Rio Blanco Oil Shale Project
Dayton Commons
9725 E. Hampden Ave.
Denver, CO 80231
Attn: K. L. Berry
D. Porter

R. Glenn Vawter
Tosco Corporation
10100 Santa Monica Blvd.
Los Angeles, CA 90067

L. L. Ludlam, Manager
Colony Development Operation
555 17th St.
P.O. Box 5300
Denver, CO 80217

Morgantotwn Energy Research Center
Box 880
Morgantown, WV 26505
Attn: W. N. Overbey, Jr.
L. A. Schrider
R. Wise
C. Komar

Continental Oil Company
P.O. Box 1267
Ponca City, OK 74601
Attn: B. G. Bray

Wayne State University
C. B. Leffert, Director
College of Engineering Energy Center
5050 Anthony Wayne Drive
Detroit, MI 48202

Dow Chemical USA
734 Building
Midland, MI 48640
Attn: C. A. Peil
L. Washington

Robert Piccirelli
Research Institute for Engineering Sciences
Wayne State University
College of Engineering
Detroit, MI 48202

John C. Koenig, Director
Commercial Development
Gulf Mineral Resources Company
1720 S. Bellaire
Denver, CO 80220

Massachusetts Institute of Technology
77 Massachusetts Ave.
Department of Mechanical Engineering
Cambridge, MA 02139
Attn: T. P. Bligh

Victor S. Englemen, Manager
Fossil Energy Sciences Division
Science Applications, Inc.
1200 Prospect St.
La Jolla, CA 92038

Suresh K. Bhatia
Booz-Allen Applied Research
4733 Bethesda Ave.
Bethesda, MD 20014

Chapman Young
Science Applications, Inc.
Steamboat Springs, CO 80477

A. E. Schlemmer, Research Advisor
Texas Eastern Transmission Corporation
P.O. Box 2521
Houston, TX 77001

Kenneth L. Ludwig, Mining Geologist
Bechtel Corporation
Engineers-Constructors
Fifty Beale St.
San Francisco, CA 94105

William L. Martin, Director
Recovery Section
Production Research Division
Research and Development Department
Continental Oil Company
P.O. Box 1267
Ponca City, OK 74601

CK Geoenergy Corporation
Suite A103, Airport Center
5030 Paradise Road
Las Vegas, NV 89119
Attn: H. Coffer
C. Boardman

Science Applications, Inc.
1546 Coal Boulevard
Golden, CO 80401
Attn: H. E. McCarthy
G. B. French
Chang-Yul Cha
R. Wise
W. J. Carter

K. P. Chong
Department of Civil and Architectural Engineering
University of Wyoming
Laramie, WY 82071
Howard Korman
TRW, Inc.
1 Space Park
R1/2112
Redondo Beach, CA 90278
The Aerospace Corporation
P.O. Box 92957
El Segundo, CA 90009
Attn: Guy F. Kuncir

INTERNAL DISTRIBUTION

G. A. Cowan, ADCELS, MS 102
H. C. Hoyt, ADEP, MS 178
L. S. Germain, DAD/AES, MS 357
R. R. Brownlee, G-DO, MS 570
B. G. Killian, G-DO, MS 570
J. Whetten, G-DO, MS 570
N. E. Vanderborgh, G-DOP, MS 329
J. W. Hopson, M-DO, MS 682
D. J. Cash, G-2, MS 978
J. L. Craig, G-2, MS 978
C. L. Edwards, G-2, MS 978
M. D. Harper, G-2, MS 978
W. R. Meadows, G-2, MS 978
R. D. Oliver, G-2, MS 978
J. M. Ray, G-2, MS 978
T. A. Weaver, G-4, MS 586
T. F. Adams, G-6, MS 665
T. Cook, G-6, MS 665
C. F. Keller, G-6, MS 665
H. N. Planner, G-6, MS 665
B. J. Travis, G-6, MS 665
J. N. Albright, G-7, MS 676
F. N. App, G-7, MS 676
E. S. Gaffney, G-7, MS 329
G. L. Schott, G-7, MS 329
M. M. Holland, LS-1, MS 880
B. Davis, M-3, MS 960
S. Goldstein, M-3, MS 960
J. R. Travis, M-3, MS 960
B. W. Olinger, M-6, MS 970
J. Shaner, M-6, MS 970
C. A. Anderson, Q-13, MS 576
K. C. Cooper, Q-13, MS 576
J. K. Dienes, T-3, MS 216
L. G. Margolin, T-3, MS 216
H. M. Ruppel, T-3, MS 216
S. A. Colgate, T-6, MS 210
J. N. Johnson, T-14, MS 214
C. L. Mader, T-14, MS 214
D. D. Eilers, X-5, MS 420
T. O. McKown, X-5, MS 420